


Switching the angular direction of radiation by the handedness of a circular dipole in the vicinity of a subwavelength Mie scatterer

Jorge R. Zurita-Sánchez ^{*}

Instituto Nacional de Astrofísica, Óptica y Electrónica, Luis Enrique Erro 1, Tonantzintla, Puebla 72840, Mexico



(Received 23 October 2020; accepted 23 March 2021; published 5 April 2021)

We study the radiation of a circular dipole nearby a subwavelength spherical particle. The circular dipole spins in a plane containing a great circle of the spherical particle (meridional plane). We derive general conditions for which radiation vanishes in any direction lying in the meridional plane, yielding directional radiation whose angular orientation can be changed by switching the handedness of the circular dipole. The radiative response (far field) of this dipole-scatterer system can be synthesized as arising from an effective electric dipole in the meridional plane and an effective magnetic dipole perpendicular to the meridional plane; both dipoles are located at the center of the sphere. We consider a nonabsorbing sphere and explore the radiative characteristics (radiation pattern, directivity, radiated power, and spin angular momentum) in which radiation is nullified along two particular axes lying in the meridional plane; particular geometrical configurations and dielectromagnetic properties of the dipole-scatterer system are given. The directional radiation and spin angular momentum patterns can be rotated π rad around the axis joining the dipole position and the center of the spherical scatterer by changing the handedness of the circular dipole, excepting for the cases of null radiation in the forward and backward directions. Our work might have implications for transferring quantum spin states to electromagnetic modes, controlling of radiation by emitters, routing of light in networks, manipulating of light propagation with metasurfaces, and sensing and locating molecules.

DOI: [10.1103/PhysRevA.103.043505](https://doi.org/10.1103/PhysRevA.103.043505)

I. INTRODUCTION

The theoretical feasibility of achieving directional scattering when a spherical particle is illuminated by a plane wave was shown in [1] (known as the Kerker effect). However, only the current technological capabilities for manufacturing and manipulating nanostructures and the development of metamaterials have allowed the experimental realization of such effect [2–5] and have opened up new possibilities for controlling the emission of light. This directional effect arises merely from the interference of radiative multipolar terms that are externally induced in a single particle or a cluster of scatterers [6–8]. Actually these scattering units are constitutive elements (meta-atoms) of metasurfaces that can be tailored for controlling light directionality [9,10]. The simultaneous interaction of azimuthally and radially polarized beams with a particle can induce a circular magnetic dipole and a linear electric dipole in which the angular direction of the radiation pattern can be modified by proper adjustment of the phase of such exciting beams [11]. Also the excitation of a nanoparticle with an azimuthally polarized beam can yield directional scattering which can be exploited for measuring displacements with angstrom resolution [12]. Moreover, the possibility of scatterers exhibiting switchable directionality has been explored; this characteristic can depend on the spectral response of dimers

[13,14], or on the polarization of an incident beam on a dimer [15] and a core-shell particle [16].

Our paper concerns to light scattering due to dipolar excitation. In this regard, the radiation arising from the interaction of an electric dipole with a metallic particle can be directed significantly in either forward or backward directions by controlling particle-emitter distance [17]. Also article [18] states the conditions for which forward or backward radiation is obtained when a linear dipole is located in the vicinity of a dielectric subwavelength sphere; the experimental verification of this directional radiation for microwaves is reported in [19]. In [20], it is described both theoretically and experimentally how the dipole excitation of a nanowire influences the radiation pattern, achieving directional emission in the forward direction. Also a directional optical antenna that is driven by a dipole can be attained by using multiple structural elements, such as a Yagi-Uda antenna [21]. Particularly for a circular dipole, depending on its helicity, its emission can be coupled to waveguide modes propagating in either the left or right direction [22–27] or to resonator modes with either positive or negative angular momentum [28,29]. In the context of quantum mechanics, the energy of molecular or atomic emitters with spin states can be directionally transferred to electromagnetic waveguide modes [30–32]. Also Raman waves with circular polarization can be coupled to plasmonic waveguides along one direction [33].

The aim of our paper is to explore whether a circular dipole in the vicinity of a subwavelength spherical particle can generate directional emission and the subsequent possibility of

^{*}jrzurita@inaoep.mx

switching the orientation of the radiative pattern by changing the handedness of such dipolar source. This effect can be crucial, as mentioned, as a transducer that converts the energy of spin states of quantum systems into radiative energy. To achieve this goal, we analyze the radiative properties (far-field) arising from the dipole-sphere emitter for establishing conditions that give rise to directional radiation. Furthermore, we examine the spin angular momentum that comes out from this antenna.

Our paper is organized as follows. Section II presents the multipolar expansion for obtaining the scattered electric field by a sphere in the presence of a circular dipole, as well as the direct electric field originating by such a dipole, and it includes the far-field asymptotics for calculating the radiation pattern, radiated power, and spin angular momentum. Three appendices complement this section. In Sec. III, for a sub-wavelength sphere, the conditions for achieving null radiation in any direction of the meridional plane (see the definition in the next section) are stated. Section IV analyzes in detail the radiative characteristics of the dipole-scatterer antenna for which radiation vanishes along two particular axes. The last section is dedicated to conclusions.

II. THEORY

We consider a spherical scatterer with radius a and center at the origin. Moreover, the sphere has dielectric and magnetic functions ϵ_2 and μ_2 , respectively. The nonabsorbing background medium has dielectric (magnetic) function ϵ_1 (μ_1); $\text{Im}[\epsilon_1] = \text{Im}[\mu_1] = 0$ ($\text{Im}[\dots]$ denotes the imaginary part). We assume that a circular electric dipole oscillates with angular frequency ω and is located outside the sphere at $\mathbf{r}_0 = z_0 \mathbf{n}_z$; $z_0 > a$ and \mathbf{n}_z is the unit Cartesian vector along the z axis. Furthermore, we consider that the dipole moment lies in the xz plane; that is,

$$\mathbf{p} = p_0[\mathbf{n}_x \pm i\mathbf{n}_z]/\sqrt{2}, \quad (1)$$

where p_0 is the strength of the dipole, \mathbf{n}_x is the unit Cartesian vector along the x axis, and the sign of (1) determines the spinning direction of the dipole. We define the meridional plane as the one containing both the dipole \mathbf{p} and a great circle of the sphere. Our setup is depicted in Fig. 1.

A. Electromagnetic field

The direct field \mathbf{E}_0 (absence of scatterer) that is created by the circular dipole can be expressed as a multipolar expansion with respect to the origin. When $|\mathbf{r}| > z_0$, this expansion is

$$\begin{aligned} \mathbf{E}_0(\mathbf{r}) = & \frac{ik_1^3}{4\pi\epsilon_0\epsilon_1} \frac{p_0}{\sqrt{2}} \sum_{l=1}^{\infty} \frac{2l+1}{l(l+1)} \left[j_l(k_1 z_0) \overline{\mathbf{M}}_{ol}(\mathbf{r}, k_1) \right. \\ & + \frac{\psi'_l(k_1 z_0)}{k_1 z_0} \overline{\mathbf{N}}_{el}(\mathbf{r}, k_1) \\ & \left. \pm il(l+1) \frac{j_l(k_1 z_0)}{k_1 z_0} \overline{\mathbf{N}}_{eo}(\mathbf{r}, k_1) \right]; \quad (2) \end{aligned}$$

the time-dependent phasor $\exp(-i\omega t)$ is hereafter omitted. Here, ϵ_0 is the vacuum permittivity, $j_l(u)$ is the spherical

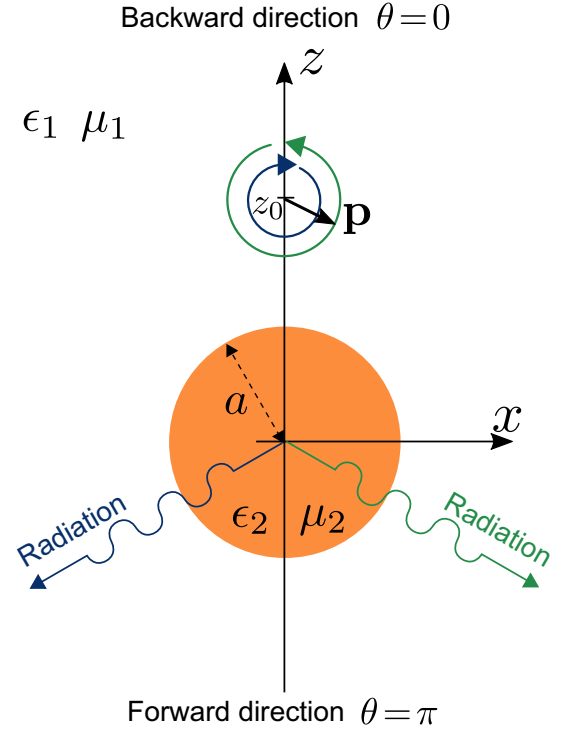


FIG. 1. Circular dipole in the vicinity a dielectromagnetic sphere. In our system, the dipole spins in the xz plane and the sphere is centered at the origin.

Bessel function of the first kind of order l , $\psi_l(u) \equiv u j_l(u)$ is the Riccati-Bessel function of order l , and $k_1 = \sqrt{\epsilon_1 \mu_1} k_0$ ($k_0 = \omega/c$; c is the light speed in vacuum) is the wave vector in the background medium. A primed function denotes the derivative with respect to its argument. The vector spherical harmonics are defined as

$$\overline{\mathbf{M}}_{\sigma lm}(\mathbf{r}, k) = \nabla \times [\mathbf{r} h_l(kr) y_{\sigma lm}(\theta, \phi)], \quad (3)$$

$$\overline{\mathbf{N}}_{\sigma lm}(\mathbf{r}, k) = \frac{1}{k} \nabla \times \overline{\mathbf{M}}_{\sigma lm}(\mathbf{r}, k), \quad (4)$$

where $\sigma = e$ and o , (r, θ, ϕ) are the spherical coordinates of \mathbf{r} , $h_l(u)$ is the spherical Hankel function of the first kind of order l , $y_{el}(\theta, \phi) \equiv P_l^m(\cos \theta) \cos(m\phi)$, and $y_{ol}(\theta, \phi) \equiv P_l^m(\cos \theta) \sin(m\phi)$; $P_l^m(\cos \theta)$ is the associated Legendre function of order m and degree l , which is explicitly defined as $P_l^m(u) \equiv (1-u^2)^{m/2} (d^m/d u^m) P_l(u)$, where $P_l(u)$ is the ordinary Legendre polynomial of order l . Equation (2) comes from the general multipolar expansion of the Green tensor [34] whose complexity is reduced when the dipolar source is located on the z axis (see details in Appendix A). Since we are only interested in the far-field region, the multipolar expansion of $\mathbf{E}_0(\mathbf{r})$ for $|\mathbf{r}| < z_0$ is omitted.

The electric field outside the spherical scatterer can be decomposed as

$$\mathbf{E}_T(\mathbf{r}) = \mathbf{E}_0(\mathbf{r}) + \mathbf{E}_1(\mathbf{r}), \quad (5)$$

where $\mathbf{E}_1(\mathbf{r})$ is the scattered electric field by the sphere. By applying Mie theory to the particular setup of Fig. 1, the

scattered electric field becomes

$$\begin{aligned} \mathbf{E}_1(\mathbf{r}) = & \frac{ik_1^3}{4\pi\epsilon_0\epsilon_1} \frac{p_0}{\sqrt{2}} \sum_{l=1}^{\infty} \frac{2l+1}{l(l+1)} \left[h_l(k_1z_0) A_l(\omega) \right. \\ & \times \bar{\mathbf{M}}_{ol1}(\mathbf{r}, k_1) + \frac{\xi'_l(k_1z_0)}{k_1z_0} B_l(\omega) \bar{\mathbf{N}}_{el1}(\mathbf{r}, k_1) \\ & \left. \pm il(l+1) \frac{h_l(k_1z_0)}{k_1z_0} B_l(\omega) \bar{\mathbf{N}}_{el0}(\mathbf{r}, k_1) \right], \quad (6) \end{aligned}$$

where $\xi_l(u) \equiv uh_l(u)$ is the Riccati-Hankel function of order l . Here, $A_l(\omega)$ and $B_l(\omega)$ are the reflection Mie coefficients which are explicitly given by

$$A_l(\omega) = \frac{\mu_2 j_l(\rho_2) \psi'_l(\rho_1) - \mu_1 j_l(\rho_1) \psi'_l(\rho_2)}{\mu_1 h_l(\rho_1) \psi'_l(\rho_2) - \mu_2 j_l(\rho_2) \xi'_l(\rho_1)}, \quad (7)$$

$$B_l(\omega) = \frac{\epsilon_2 j_l(\rho_2) \psi'_l(\rho_1) - \epsilon_1 j_l(\rho_1) \psi'_l(\rho_2)}{\epsilon_1 h_l(\rho_1) \psi'_l(\rho_2) - \epsilon_2 j_l(\rho_2) \xi'_l(\rho_1)}, \quad (8)$$

where $\rho_i = k_i a$ ($i = 1, 2$ and $k_2 = \sqrt{\epsilon_2 \mu_2} k_0$). The analytical expression (6) comes from general multipolar series of the scattering Green tensor [35]; similarly to the case of the direct field, the dipole position lying in the z axis simplifies the multipolar expansion of such a Green tensor as shown in Appendix A.

B. Far-field limit

To calculate the scattered field in the radiation zone, we use the asymptotic expressions for the spherical Hankel and Riccati-Hankel functions:

$$\lim_{\rho \rightarrow \infty} h_l(\rho) = e^{i\rho} / (i^{l+1} \rho), \quad \lim_{\rho \rightarrow \infty} \rho^{-1} \xi'_l(\rho) = e^{i\rho} / (i^l \rho). \quad (9)$$

By using (9) in (6) and (2), the far-field limit of the electric field $\mathbf{E}_T(\mathbf{r})$ becomes

$$\begin{aligned} \mathbf{E}_{T\infty}(\mathbf{r}) = & \frac{k_1^2}{4\pi\epsilon_0\epsilon_1} \frac{ie^{ik_1r}}{r} \frac{p_0}{\sqrt{2}} \sum_{l=1}^{\infty} \frac{1}{i^l} \frac{2l+1}{l(l+1)} \left[\frac{\alpha_l(k_1z_0)}{i} \right. \\ & \times \mathbf{P}_{ol1}(\theta, \phi) + \beta_l(k_1z_0) \mathbf{Q}_{el1}(\theta, \phi) \\ & \left. \pm il(l+1) \gamma_l(k_1z_0) \mathbf{Q}_{el0}(\theta, \phi) \right], \quad (10) \end{aligned}$$

where

$$\alpha_l(\rho) = j_l(\rho) + h_l(\rho) A_l(\omega), \quad (11)$$

$$\beta_l(\rho) = [\psi'_l(\rho) + B_l(\omega) \xi'_l(\rho)] / \rho, \quad (12)$$

$$\gamma_l(\rho) = [j_l(\rho) + B_l(\omega) h_l(\rho)] / \rho, \quad (13)$$

and

$$\mathbf{P}_{o_{lm}}^e(\theta, \phi) = \mp \Pi_l^m(\theta) m \frac{\sin(m\phi)}{\cos(m\phi)} \mathbf{n}_\theta - \tau_l^m(\theta) \frac{\cos(m\phi)}{\sin(m\phi)} \mathbf{n}_\phi, \quad (14)$$

$$\mathbf{Q}_{o_{lm}}^e(\theta, \phi) = \mathbf{n}_r \times \mathbf{P}_{o_{lm}}^e(\theta, \phi); \quad (15)$$

$$\tau_l^m(\theta) = \frac{d}{d\theta} P_l^m(\cos\theta), \quad (16)$$

$$\Pi_l^m(\theta) = \frac{P_l^m(\cos\theta)}{\sin\theta}. \quad (17)$$

Here, \mathbf{n}_r , \mathbf{n}_θ , and \mathbf{n}_ϕ are the unit spherical vectors. The magnetic field in the radiation zone is

$$\begin{aligned} \mathbf{H}_{T\infty}(\mathbf{r}) = & \frac{k_1^2}{4\pi\epsilon_0\epsilon_1 Z_1} \frac{e^{ik_1r}}{r} \frac{p_0}{\sqrt{2}} \sum_{l=1}^{\infty} \frac{1}{i^l} \frac{2l+1}{l(l+1)} \left[\alpha_l(k_1z_0) \right. \\ & \times \mathbf{Q}_{ol1}(\theta, \phi) + \frac{\beta_l(k_1z_0)}{i} \mathbf{P}_{el1}(\theta, \phi) \\ & \left. \pm l(l+1) \gamma_l(k_1z_0) \mathbf{P}_{el0}(\theta, \phi) \right], \quad (18) \end{aligned}$$

where $Z_1 = [(\mu_0 \mu_1) / (\epsilon_0 \epsilon_1)]^{1/2}$ is the impedance of the background medium.

C. Radiated power

The time-average far-field Poynting vector is

$$\langle \mathbf{S}(\mathbf{r}, t) \rangle = \frac{1}{2} \text{Re}[\mathbf{E}_{T\infty}^*(\mathbf{r}) \times \mathbf{H}_{T\infty}(\mathbf{r})], \quad (19)$$

where $\text{Re}[\dots]$ denotes the real part. Then, the radiated power, namely, the energy flux that goes through a large sphere with radius R , is

$$P = \int_A \frac{dP(\theta, \phi)}{d\Omega} d\Omega, \quad (20)$$

where $d\Omega$ is the solid angle differential and

$$\frac{dP(\theta, \phi)}{d\Omega} = \langle \mathbf{S}(R, \theta, \phi) \rangle \cdot \mathbf{n}_r R^2 \quad (21)$$

is the so-called radiation pattern. Then, the radiation pattern can be expressed as a sum of multipolar contributions:

$$\frac{1}{P_0} \frac{dP}{d\Omega} = \sum_{l,l'} \frac{1}{P_0} \frac{dP_{ll'}}{d\Omega}, \quad (22)$$

where $P_0^{-1}(dP_{ll'}/d\Omega)$ is explicitly defined in Appendix B. The radiated power turns out to be

$$\frac{P}{P_0} = \sum_{l=1}^{\infty} \frac{P_l}{P_0}, \quad (23)$$

where

$$\begin{aligned} \frac{P_l}{P_0} = & \frac{3}{4} \frac{(2l+1)}{2} [|\alpha_l(k_1z_0)|^2 + |\beta_l(k_1z_0)|^2 \\ & + 2l(l+1) |\gamma_l(k_1z_0)|^2]. \quad (24) \end{aligned}$$

Here, P_0 is the radiated power by a dipole when the scatterer is absent, which is given by

$$P_0 = \frac{1}{3} \frac{\omega k_1^3 |p_0|^2}{4\pi\epsilon_0\epsilon_1}. \quad (25)$$

We mention that (23) is obtained by using the orthogonal properties of spherical harmonics [36].

D. Spin angular momentum

The spin angular momentum density is [37]

$$\mathbf{s}(\mathbf{r}) = \frac{1}{4\omega} \text{Im}[\varepsilon_0 \epsilon_1 \mathbf{E}^*(\mathbf{r}) \times \mathbf{E}(\mathbf{r}) + \mu_0 \mu_1 \mathbf{H}^*(\mathbf{r}) \times \mathbf{H}(\mathbf{r})]. \quad (26)$$

This quantity is related to circular polarization of light and can be related to the Stokes parameters [38]. In the radiation zone, that is, $k_1 r \gg 1$, the spin angular momentum density becomes

$$\mathbf{s}_\infty(\mathbf{r}) = \frac{\mathbf{n}_r}{r^2} \tilde{s}(\theta, \phi), \quad (27)$$

where \tilde{s} is denominated hereafter as the *spin pattern* whose multipolar decomposition is

$$\tilde{s}(\theta, \phi) = \sum_{l,l'=1}^{\infty} \tilde{s}_{ll'}(\theta, \phi) \quad (28)$$

(the explicit analytical expression of $s_{ll'}$ is found in Appendix C). Here, \mathbf{s}_∞ comes from (26) in which the far-field approximations of the electric and magnetic fields [(10) and (18), respectively] are substituted.

III. DIRECTIONAL SUBWAVELENGTH RESPONSE

When $k_1 a \ll 1$, that is, a subwavelength particle, we expect that the dipolar response of the sphere comes mainly from the dipolar order ($l = 1$). Then, up to $l = 1$, the far-field electric field can be synthesized as arising from an effective magnetic dipole oriented in the y direction ($\mathbf{m}_{\text{ef}} = m_y \mathbf{n}_y$; \mathbf{n}_y is the unit vector along the y axis), and an effective electric dipole which is polarized in the xz plane ($\mathbf{p}_{\text{ef}} = p_x \mathbf{n}_x + p_z \mathbf{n}_z$), that is,

$$\mathbf{E}_{T\infty}(\mathbf{r}) = \frac{k_1^2}{4\pi \varepsilon_0 \epsilon_1} \frac{e^{ik_1 r}}{r} \{ [\cos \theta \cos \phi \mathbf{n}_\theta - \sin \phi \mathbf{n}_\phi] p_x + [\cos \phi \mathbf{n}_\theta - \cos \theta \sin \phi \mathbf{n}_\phi] (m_y n_1 / c) - \sin \theta \mathbf{n}_\theta p_z \}, \quad (29)$$

where $n_1 = \sqrt{\epsilon_1 \mu_1}$ is the refractive index of background medium and the effective dipoles are

$$m_y n_1 / c = \frac{\alpha_1(k_1 z_0)}{i} \frac{3p_0}{2\sqrt{2}}, \quad (30)$$

$$p_x = \beta_1(k_1 z_0) \frac{3p_0}{2\sqrt{2}}, \quad (31)$$

$$p_z = \pm 2i \gamma_1(k_1 z_0) \frac{3p_0}{2\sqrt{2}}. \quad (32)$$

The radiation pattern arising from these dipoles is

$$\begin{aligned} \frac{1}{P_x} \frac{dP_{11}}{d\Omega} &= \frac{3}{8\pi} [(1 - \sin^2 \theta \cos^2 \phi) + f_2^2 \sin^2 \theta \\ &+ f_1^2 (1 - \sin^2 \theta \sin^2 \phi) + 2f_1 \cos \theta \cos \delta_1 \\ &- 2f_2 \sin \theta \cos \theta \cos \phi \cos \delta_2 \\ &- 2f_1 f_2 \sin \theta \cos \phi \cos(\delta_1 - \delta_2)]. \end{aligned} \quad (33)$$

Here, P_x is radiated power by the effective dipole p_x embedded in the background medium, namely,

$$P_x = \frac{1}{3} \frac{\omega k_1^3 |p_x|^2}{4\pi \varepsilon_0 \epsilon_1}, \quad (34)$$

and we have defined

$$f_1 \exp(i\delta_1) = m_y n_1 / (p_x c), \quad f_2 \exp(i\delta_2) = p_z / p_x, \quad (35)$$

namely, f_1 and f_2 (δ_1 and δ_2) are the magnitudes (arguments) of $m_y n_1 / c$ and p_z normalized with respect to p_x , respectively. To avoid further confusion, we emphasize that parameters f_1 , δ_1 , f_2 , and δ_2 concern to effective dipoles, while the dipolar source or circular dipole refers to the physical source (1).

The spin pattern due to the lowest order becomes

$$\begin{aligned} \tilde{s}_{11}(\theta, \phi) &= \tilde{s}_x \sin \theta \sin \phi [f_1 \sin \theta \cos \phi \sin \delta_1 \\ &- f_2 \sin \delta_2 + f_1 f_2 \cos \theta \sin(\delta_1 - \delta_2)], \end{aligned} \quad (36)$$

where $\tilde{s}_x = 3n_1 P_x / (4\pi c \omega)$. We can notice that the first, second, and third term of the right-hand side of (36) correspond to the spin angular momentum that is generated by the mixing of effective dipoles $p_x - m_y$, $p_x - p_z$, and $p_z - m_y$, respectively. Also, (36) indicates that the \tilde{s}_{11} vanishes in any directional vector that lies in the meridional plane.

We define a unit vector in the xz plane as

$$\mathbf{n}_d = \sin \psi \mathbf{n}_x + \cos \psi \mathbf{n}_z, \quad (37)$$

where ψ is angle between the z axis and \mathbf{n}_d . To attain null radiation in a direction perpendicular to the plane expanded by unit vectors \mathbf{n}_d and \mathbf{n}_y , the Huygens' dipole condition, which gives rise to directional radiation, must be fulfilled, namely,

$$\mathbf{n}_d \cdot \mathbf{p}_{\text{ef}} = \pm m_y n_1 / c. \quad (38)$$

Hence it is possible to nullify the radiation in any direction along the meridional plane.

Importantly, the ratio of effective dipoles p_z / p_x is proportional to $\gamma_1(k_1 z_0) / \beta_1(k_1 z_0)$ which is real for nonabsorbing dielectromagnetic materials. We restrict ourselves hereafter to these kinds of materials; thus

$$\delta_2 = \pm (\pi/2) \text{sgn}[\gamma_1(k_1 z_0) / \beta_1(k_1 z_0)], \quad (39)$$

where $\text{sgn}[\dots]$ is the sign function and the \pm signs come from the handedness of the circular dipole [see (1)]. Hence, on one hand, the positive sign of the right-hand side of (38) yields conditions

$$f_1^2 = \sin^2 \psi + f_2^2 \cos^2 \psi, \quad (40)$$

$$\delta_1 = \arctan(\sin \psi, \text{sgn}[\delta_2] f_2 \cos \psi), \quad (41)$$

and the null-radiation direction is $\mathbf{n}_0^+ = \cos \psi \mathbf{n}_x - \sin \psi \mathbf{n}_z$; $\arctan(u, v)$ is defined as $\arctan(v/u)$ in which the quadrant of point (u, v) is taken into account. On the other hand, for the solution corresponding to the negative sign of the right-hand side of (38), the relation between f_1 and f_2 is the same as (40),

$$\delta_1 = \pi + \arctan(\sin \psi, \text{sgn}[\delta_2] f_2 \cos \psi), \quad (42)$$

and $\mathbf{n}_0^- = -\cos \psi \mathbf{n}_x + \sin \psi \mathbf{n}_z$ is the direction for which radiation vanishes. Therefore, (39)–(42) are the conditions in which radiation can vanish in any direction that lies in the meridional plane, yielding a directional radiation pattern.

Relative to the meridional plane (xz plane), the radiation pattern is symmetric, while the spin pattern is antisymmetric (sign change). Furthermore, by considering the aforementioned condition $\delta_2 = \pm \pi/2$, the change of the dipolar source handedness rotates the radiation and spin patterns π rad

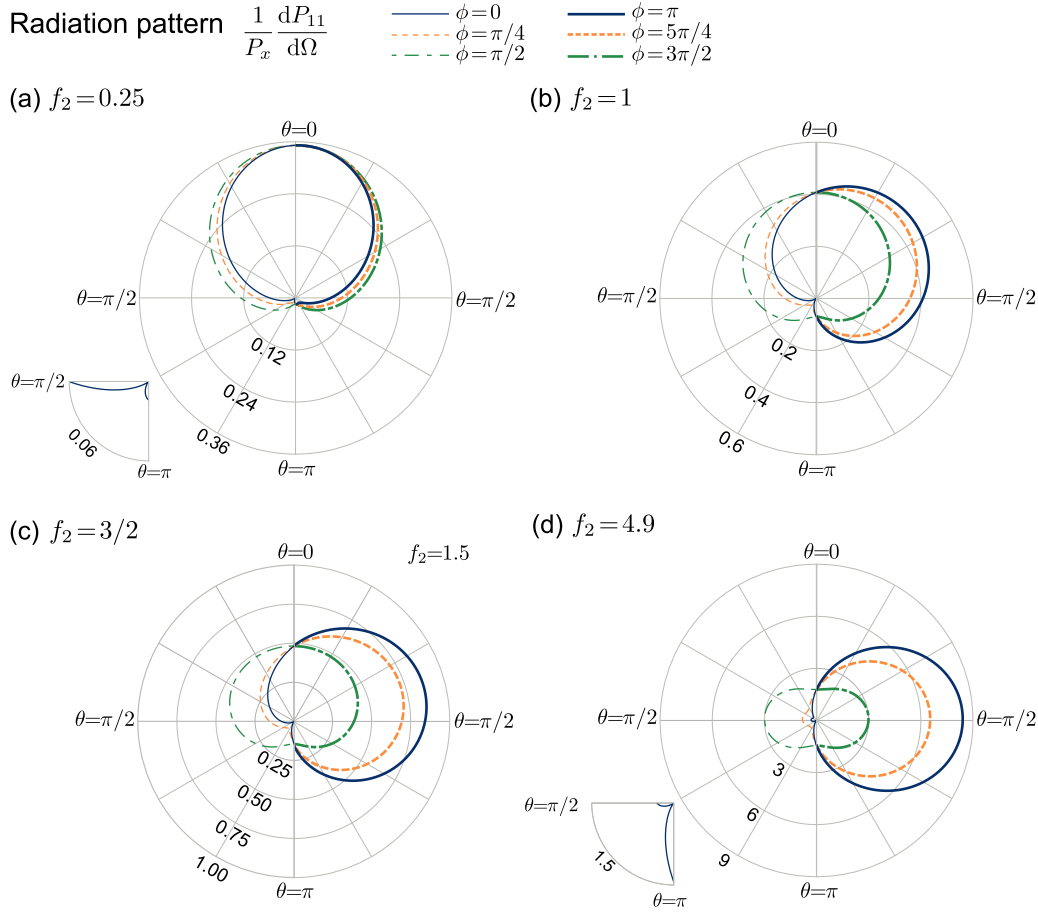


FIG. 2. Radiation pattern $P_x^{-1}dP_{11}/d\Omega$ for $f_2 = 0.25, 1, 1.5,$ and $f = 4.29$. Radiation vanishes in the direction $(\mathbf{n}_x - \mathbf{n}_z)/\sqrt{2}$.

around the z axis, explaining the shift of the angular direction of radiation. These symmetric properties of the radiation and spin patterns can be seen by replacing $\sin \theta \cos \phi \rightarrow x/r,$ $\sin \theta \sin \phi \rightarrow y/r,$ and $\cos \theta \rightarrow z/r$ in (33) and (36).

IV. RESULTS

As illustrative cases, we analyze the radiative characteristics that occur along two particular axes lying in the meridional plane (xz plane), where the radiation vanishes unidirectionally. The first axis is $z = x$ (or axis $z = -x$ which is indeed correlated with axis $z = x$) and is denominated as the “diagonal axis.” The second of them is the principal axis which is the line passing through the circular dipole position and the center of the sphere (z axis); it defines the conventional backward ($\theta = 0$) and forward ($\theta = \pi$) directions.

A. Diagonal axis

In this case, $\psi = \pi(1/4 + q/2)$ ($q = 0, 1, 2, 3$). Consequently, $f_1^2 = (1 + f_2^2)/2$ and $\delta_1 = \pm \arctan(f_2), \pi \pm \arctan(f_2)$; the value of δ_1 depends on angle $\psi,$ the sign of $\delta_2,$ and the sign of the right-hand side of (38). Then, the radiation pattern in terms of f_2 is

$$\frac{1}{P_x} \frac{dP_{11}}{d\Omega} = \frac{3}{8\pi} [1 - \text{sgn}[\mathbf{n}_0^\pm \cdot \mathbf{n}_z] \sqrt{2} \cos \theta - \text{sgn}[\mathbf{n}_0^\pm \cdot \mathbf{n}_x] \sqrt{2} f_2^2 \sin \theta \cos \phi$$

$$+ f_2^2 \sin^2 \theta - \sin^2 \theta \cos^2 \phi + (1 + f_2^2)(1 - \sin^2 \theta \sin^2 \phi)/2], \quad (43)$$

whereas the spin pattern turns out be

$$\tilde{s}_{11}(\theta, \phi) = \tilde{s}_x f_2 \sin \theta \sin \phi \text{sgn}[\delta_2] [-1 + (\sqrt{2}/2) \text{sgn}[\mathbf{n}_z \cdot \mathbf{n}_0^\pm] \cos \theta + (\sqrt{2}/2) \text{sgn}[\mathbf{n}_x \cdot \mathbf{n}_0^\pm] \sin \theta \cos \phi]. \quad (44)$$

As an example, we consider $\psi = \pi/4$ and the condition with the positive sign of the right-hand side of (38); thus $\mathbf{n}_0^+ = (\mathbf{n}_x - \mathbf{n}_z)/\sqrt{2}$. These parameters yield the radiation patterns for several values of f_2 that are depicted in Fig. 2. When $f_2 < 0.2873,$ the maximum of the radiation pattern occurs at $\theta_m = 0,$ as seen in Fig. 2(a). For this case, the contribution of the effective dipole $p_z,$ in comparison to the others, is small; thus the radiation pattern is mainly directed in the forward direction and it depends weakly on $\phi.$ However, as is shown in the zoomed region of Fig. 2(a), the radiation vanishes in the direction $(\theta = 3\pi/4, \phi = 0).$ When $f_2 > 0.2873,$ the maximum of the radiation pattern occurs at $\phi_m = \pi$ and θ_m obeys $f_2^2 \cos \theta_m (\sqrt{2} + 2 \sin \theta_m) - \sin \theta_m (\sqrt{2} + 2 \cos \theta_m) = 0.$ For $f_2 = 1,$ $\theta_m = \pi/4$ and this direction is exactly the opposite of \mathbf{n}_0^+ [see Fig. 2(b)]. In Fig. 2(c) ($f_2 = 3/2$), the angle θ_m increases to $0.421\pi.$ As f_2 grows even more, the effective dipoles p_z and m_y are much

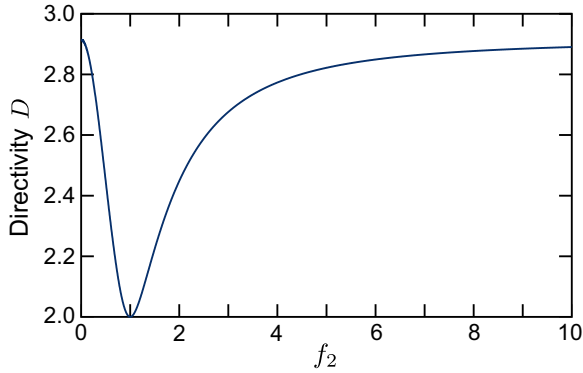


FIG. 3. Directivity D as a function of f_2 when radiation is nullified along any of four directions $(\pm \mathbf{n}_x \pm \mathbf{n}_z)/\sqrt{2}$.

greater than effective dipole p_x and $\theta_m \rightarrow \pi/2$. Consequently, directional radiation of the scatterer-dipole antenna occurs predominantly along the negative x axis and null radiation is still maintained in direction \mathbf{n}_0^+ ; this is seen in Fig. 2(d) for $f_2 = 4.9$.

The directivity D as a function of f_2 is plotted in Fig. 3. The directivity D is defined as

$$D^{-1} = \frac{1}{4\pi} \frac{1}{\max[dP(\theta, \phi)/d\Omega]} \int \frac{dP(\theta, \phi)}{d\Omega} d\Omega, \quad (45)$$

where $\max[\dots]$ denotes the maximum. We can notice that the directivity is bounded in the interval $2 < D < (3 + 2\sqrt{2})/2$; the superior limit happens when $f_2 \rightarrow 0$ or $f_2 \rightarrow \infty$, whereas $f_2 = 1$ yields the inferior limit. The radiated power is

$$\frac{P_1}{P_x} = \frac{3}{2}(1 + f_2^2). \quad (46)$$

Again, we assume $\psi = \pi/4$ and the condition with the positive sign of the right-hand side of (38), obtaining the spin pattern that is illustrated in Fig. 4. As can be noticed from (44), the shape of the spin angular momentum pattern is independent of factor f_2 , but this factor scales linearly the strength of this pattern. The maximum strength of this pattern occurs when $\theta_m = \arccos[1/(2\sqrt{2})]$ and $\phi_m = \pi - \arccos[1/(\sqrt{7})]$.

Now we present a narrow subset of material and geometric parameters of the dipole-scatterer antenna that render the aforementioned directional far-field response: null radiation along directions $\pm \mathbf{n}_x - \mathbf{n}_z$ (the direction is set by the spinning direction of the dipolar source). The background medium is hereafter vacuum ($\epsilon_1 = \mu_1 = 1$, $k_1 = k_0$). We consider two normalized sizes of the scatterer ($k_0 a = 0.3$ and 0.35). Figure 5(a) shows the dielectric and magnetic functions of the particle as the surface-source separation $k_0(z_0 - a)$ varies for which the aforementioned conditions for directional radiation are fulfilled. As seen, ϵ_2 (μ_2) increases (decreases) as the separation $k_0(z_0 - a)$ increases. Also, for a fixed value of surface-source separation, the dielectric and magnetic functions (ϵ_2 and μ_2 , respectively) are larger for the smaller particle. At first instance, we notice that materials possessing those values of ϵ_2 and μ_2 might not exist. However, we expect that metamaterials with simultaneously large effective permittivity and permeability would be realizable [39–41]. Also we mention that the aforementioned conditions are exactly

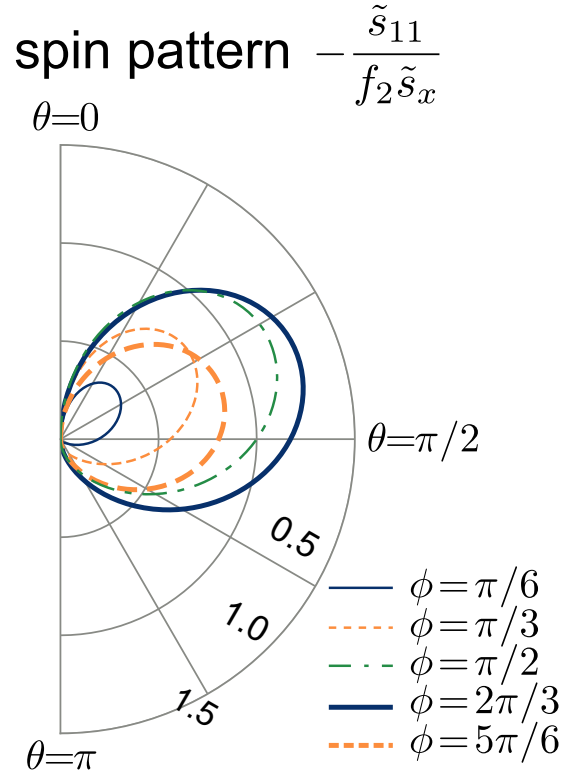


FIG. 4. Spin pattern $\tilde{s}_{11}/(f_2 \tilde{s}_x)$ for $\phi = \pi/6, \pi/3, \pi/2, 2\pi/3$, and $5\pi/6$. Radiation vanishes in the direction $(\mathbf{n}_x - \mathbf{n}_z)/\sqrt{2}$.

matched, so if these conditions are approximately satisfied, then the dielectromagnetic properties of metamaterials might be tailored with less difficulty. Another possibility is to explore the dipolar response of a multilayered spherical particle which might ease the material limitations. For those parameters of Fig. 5(a), Fig. 5(b) illustrates the strength of the ratio of the effective electric dipoles p_z and p_x (f_2), and the relative phase difference δ_1 between the effective magnetic m_y and electric dipoles against the normalized separation $k_0(z_0 - a)$; the strength f_1 depends on f_2 [see (40)] and $\delta_2 = \pm \pi/2$ [see (39)].

We consider specifically a sphere with radius $k_0 a = 0.3$, $\epsilon_2 = 12.2458$, and $\mu_2 = 16$. Moreover, the circular dipole is located at $k_0 z_0 = 0.3812$. These factors fulfill (40) and (41) with $\psi = \pi/4$ and $\delta_2 = -\pi/2$ (the upper sign of (1) is considered since $\text{sgn}[\gamma_1/\beta_1] = -1$), yielding $f_1 = 1.2741$, $\delta_1 = -0.3127\pi$, and $f_2 = 1.499$. Consequently, the radiation pattern corresponds to the one of Fig. 2(c). The radiated power from the lowest multipole is $P_1 = 4.8704P_x = 39.6223P_0$. To quantify the impact of high-order multipoles on the radiation pattern, we calculate the error as

$$\sigma_p = \frac{1}{P_x} \left| \frac{dP_{11}}{d\Omega} - \frac{dP}{d\Omega} \right|. \quad (47)$$

As seen in Fig. 6(a), the contribution of high-order multipoles practically unperturbs the radiation pattern since the error σ_p is much smaller than the strength of the radiation pattern of the lowest order [compare Figs. 6(a) and 2(c)]. In addition, the contribution of high-order multipoles to the radiated power with respect to total radiated power is about

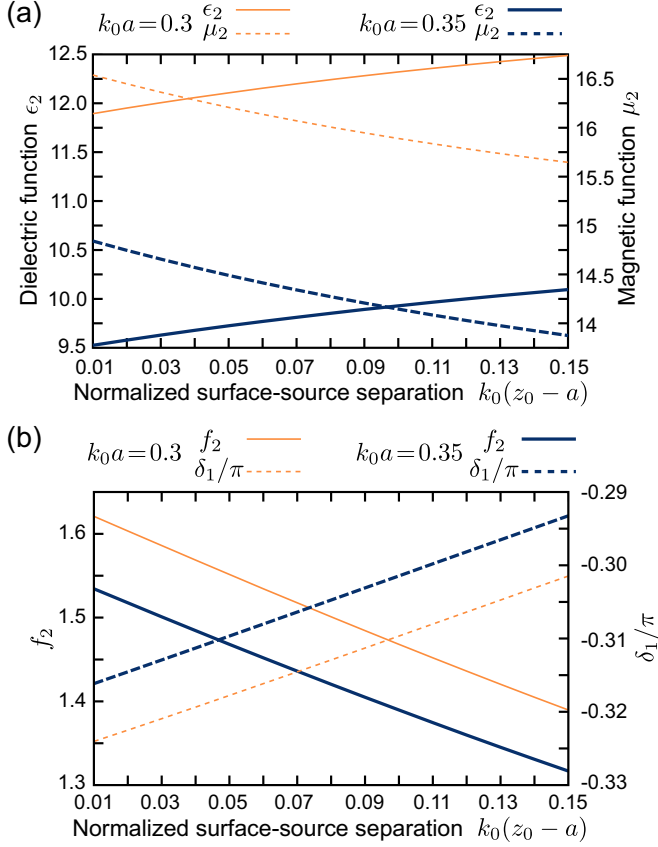


FIG. 5. (a) ϵ_2 (left axis) and μ_2 (right axis) fulfilling condition of directional radiation along the diagonal axis versus the surface-dipole separation $k_0(z_0 - a)$ for $k_0a = 0.3$ and 0.35 . (b) The strength f_2 (left axis) and phase δ_1 (right axis) versus the surface-dipole separation $k_0(z_0 - a)$ that arises from material parameters ϵ_2 and μ_2 and particle size k_0a of panel (a).

0.094%. Concerning the spin angular momentum pattern, the lowest order contribution, \tilde{s}_{11} , matches exactly the one that is shown in Fig. 4. Like the radiation pattern, the contribution of high-order multipoles to the spin angular momentum pattern has almost no impact. This is seen in Fig. 6(b) where the spin error, which is defined as

$$\sigma_s = \frac{1}{f_2 \tilde{s}_x} |\tilde{s}_{11}(\theta) - \tilde{s}(\theta, \phi)|, \quad (48)$$

is plotted; the error σ_s is negligible in comparison with the dipolar part of the strength of the spin pattern [see Figs. 4 and 6(b)].

As mentioned, if the handedness of the circular dipole is changed [the lower sign of (1)], then $\delta_2 = \pi/2$ and the radiation pattern is the same as that of Fig. 2(c), but $\phi \rightarrow \phi + \pi$ [null-radiation is directed along unit vector $-(\mathbf{n}_x + \mathbf{n}_z)/\sqrt{2}$]; conditions (40) and (41) with $\psi = 3\pi/4$ are satisfied and factors f_1 , δ_1 , and f_2 are unchanged. Therefore, by changing the spinning direction of the circular dipole, the directionality of the antenna can be switched.

Now we concisely consider another particular case for which the radiation direction can be nullified in the upper half-space ($z > 0$). With $\psi = 3\pi/4$ and the negative sign of the right-hand side of (38), the direction in which the

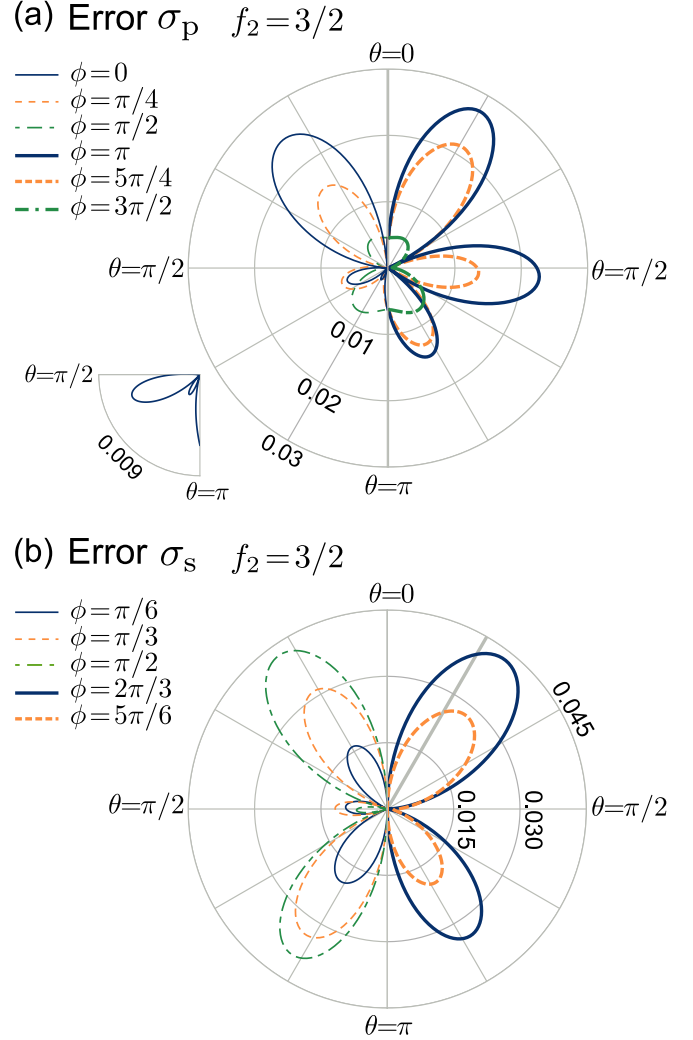


FIG. 6. The setup has parameters $k_0a = 0.3$, $\epsilon_2 = 12.2458$, $\mu_2 = 16$, and $k_0z_0 = 0.3812$; $f_2 = 1.499$; radiation vanishes in directions $(\pm \mathbf{n}_x - \mathbf{n}_z)/\sqrt{2}$. (a) Radiation pattern error σ_p . (b) Spin pattern error σ_s .

radiation vanishes is $\mathbf{n}_0^- = (\mathbf{n}_x + \mathbf{n}_z)/\sqrt{2}$. By assuming $\delta_2 = \pi/2$ (the lower sign of (1) is considered since $\text{sgn}[\gamma_1/\beta_1] = -1$), the following parameters satisfy (40) and (42): $k_0a = 0.3$, $k_0z_0 = 0.3111$, $\epsilon_2 = 18.0785$, and $\mu_2 = 10$; they render $f_1 = 3.5386$, $\delta_1 = 0.5639\pi$, and $f_2 = 4.9033$. For this case, the radiation pattern and spin patterns are obtained by applying a reflection transformation with respect to the xy plane to Fig. 2(d) and Fig. 4. The radiated power turns out to be $P_1 = 37.5629P_x = 25.175P_0$. Similarly to the previous case, the dipolar contribution of the radiation and spin patterns is much stronger than any other corresponding high-order multipolar term. As explained, the change of rotation direction of the dipolar source to $\delta_2 = -\pi/2$ switches the null-radiation direction to $\mathbf{n}_0^- = (-\mathbf{n}_x + \mathbf{n}_z)/\sqrt{2}$.

B. Principal axis

Now we examine the case in which null radiation is attained in either the forward or backward direction in the presence of the circular dipole. According to the

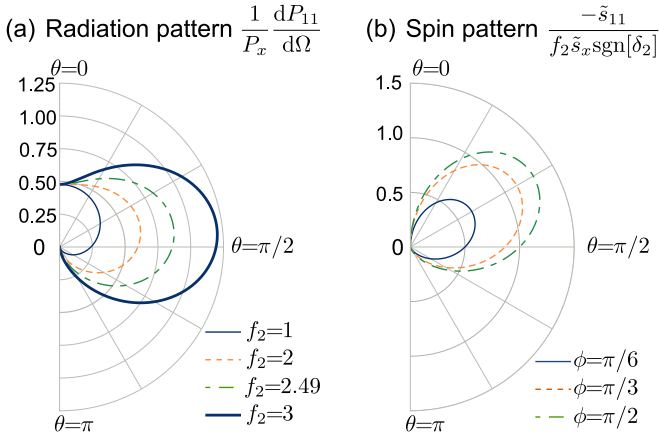


FIG. 7. (a) Radiation pattern $P_x^{-1} dP_{11}/d\Omega$ for $f_2 = 1, 2, 2.49$, and 3 . (b) Spin pattern $-\tilde{s}_{11}/(f_2 \tilde{s}_x \text{sgn}[\delta_2])$ for $\phi = \pi/6, \pi/3$, and $\pi/2$. Radiation vanishes in the forward direction.

aforementioned conditions, the radiation pattern cannot be switched by flipping the rotation direction of the dipolar source.

First we analyze the case in which radiation in the forward direction is obtained. This happens when $\psi = \pi/2$ ($3\pi/2$) for the positive (negative) sign of the right-hand side of (38). As a consequence $\delta_1 = 0$, $f_1 = 1$, and $\delta_2 = \pm\pi/2$ (as expected the null-forward radiation is independent of the spinning direction of the circular dipole). Then, from (33), the radiation pattern becomes

$$\frac{1}{P_x} \frac{dP_{11}}{d\Omega} = \frac{3}{8\pi} [(1 + \cos \theta)^2 + f_2^2 \sin^2 \theta], \quad (49)$$

which is independent of the azimuthal angle ϕ . Although f_2 has no impact in the aforementioned condition of null radiation, it affects the radiation pattern. This can be shown in Fig. 7(a) in which the radiation pattern for several values of f_2 is plotted. On one hand, if $f_2 \leq \sqrt{2}$, the maximum of $P_x^{-1} dP_{11}/d\Omega$ is $3/(2\pi)$ and occurs when $\theta = 0$, as illustrated in Fig. 7(a) for $f_2 = 1$. In the limit $f_2 \rightarrow 0$, the conventional Huygens dipole is attained. On the other hand, when $f_2 > \sqrt{2}$, the angle $\cos \theta_m = (f_2^2 - 1)^{-1}$ gives the maximum of $P_x^{-1} dP_{11}/d\Omega$ which is equal to $3f_2^4/[8\pi(f_2^2 - 1)]$. Consequently, as shown in Fig. 7(a), as f_2 becomes larger, $\theta_m \rightarrow \pi/2$, meaning that the radiation lobe builds up perpendicularly in relation to the dipole orientation. The directivity D of the antenna is

$$D = \begin{cases} 6/(2 + f_2^2), & f_2 \leq \sqrt{2}, \\ 3f_2^4/[2(2 + f_2^2)(f_2^2 - 1)], & f_2 > \sqrt{2}, \end{cases} \quad (50)$$

and it is plotted in Fig. 8. We can notice that the factor f_2 controls the antenna directivity. As seen in Fig. 8, at $f_2 = 0$, D is maximal and has a value of 3 . Then, D decreases to the minimum level of $4/3$ when $f_2 = 2$ and $D = 3/2$ as $f_2 \rightarrow \infty$ (the directivity of a dipole embedded in a background medium is equal to this value). The radiated power P becomes

$$P_1/P_x = 2 + f_2^2. \quad (51)$$

The spin pattern reduces to

$$\tilde{s}_{11}(\theta, \phi) = -\tilde{s}_x f_2 \text{sgn}[\delta_2] \sin \theta \sin \phi (1 + \cos \theta), \quad (52)$$

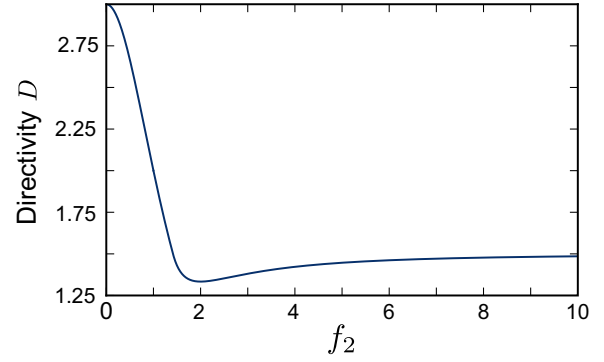


FIG. 8. Directivity D as a function of f_2 when radiation vanishes in either backward or forward direction.

and it is depicted in Fig. 7(b). It can be seen from (52) that phase δ_2 determines spin angular moment direction. Like the diagonal-axis case, the shape of the angular spin pattern is independent of f_2 (this parameter acts only as a scaling factor). The maximal strength of the angular spin pattern occurs when $\theta_m = \pi/3$ and $\phi_m = \pi/2$.

Now we discuss a particular configuration of the dipole-scatterer system that yields the aforementioned radiative patterns. We consider a sphere with size $k_0 a = 0.3$ and a circular dipole located at $k_0 z_0 = 0.35$. We look for values of ϵ_2 and μ_2 which fulfill the aforementioned conditions for achieving no radiation in the forward direction. We find that such conditions are met when $\epsilon_2 = 13.386$ and $\mu_2 = 14.542$, yielding $f_2 = 2$. The radiation pattern of the dipolar contribution ($l = 1$) of the dipole-sphere antenna matches exactly the radiation pattern of Fig. 7(a) with $f_2 = 2$. There are high-order contributions to the radiation and spin angular patterns; however these contributions perturb slightly those patterns. This is indeed shown in Fig. 9 where the errors σ_p and σ_s are plotted for several values of ϕ . As seen the errors σ_p and σ_s are much smaller than the strengths $P_x^{-1} dP_{11}/d\Omega$ and $|\tilde{s}_{11}/(f_2 \tilde{s}_x)|$, respectively. The total radiated power due to the dipolar contribution is $P_1 = 6P_x = 449.8126P_0$, whereas the

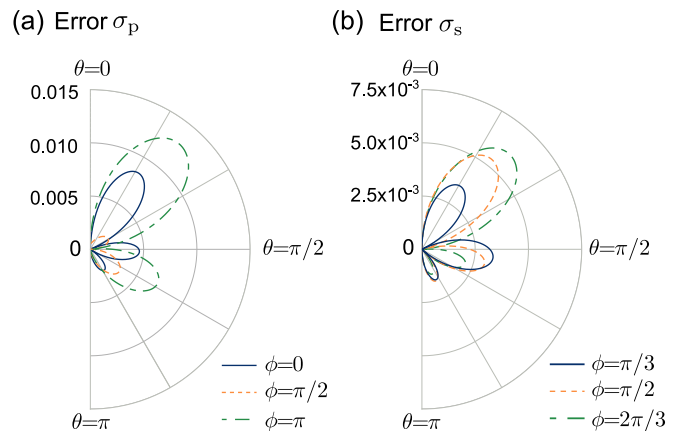


FIG. 9. Case of vanishing radiation in the forward direction. (a) Radiation pattern error σ_p . (b) Spin pattern error σ_s . $k_0 a = 0.3$, $k_0 z_0 = 0.35$, $\epsilon_2 = 13.386$, $\mu_2 = 14.542$, and $f_2 = 2$.

addition of all multipoles yields $P = 449.8522P_0$; this shows as well the low impact of higher order multipoles.

Opposite to previous case, the radiation is nullified in the backward direction when $\psi = 3\pi/2$ ($\pi/2$) for the positive (negative) sign of the right-hand side of (38). Hence, $\delta_1 = \pi$ and again $f_1 = 1$ and $\delta_2 = \pm\pi/2$. The reflection of the radiation and spin patterns of Fig. 7 with respect to the xy plane renders those corresponding to case of zero radiation in the backward direction. Hence, these patterns exhibit the same characteristics of those corresponding to the null-forward direction. Again we consider a dielectromagnetic sphere with size $k_0a = 0.3$ and a circular dipole located at $k_0z_0 = 0.35$. We find that the sphere with $\epsilon_2 = 14.435$ and $\mu_2 = 13.373$ fulfills the aforementioned conditions for null radiation in the backward direction with $f_2 = 2.49$. As mentioned, the radiation and spin patterns of the dipolar contribution coincide exactly with the one of Fig. 7(a) with $f_2 = 2.49$ and Fig. 7(b), respectively (after performing the xy -plane reflection). Similarly to the previous case, almost imperceptible deviations from the dipolar radiation pattern are caused by high-order multipoles. The radiated power from the dipolar order is $P_1 = 8.2P_x = 579.94P_0$, and the total radiated power that includes all multipoles is $P = 579.98P_0$ which is only a few hundredths of P_0 larger than that of the dipolar part.

V. CONCLUSIONS

We studied the electromagnetic response in the far field of a circular electric dipole placed near a subwavelength sphere; the circular dipole spins in a plane containing a great circle of the sphere (meridional plane). The aforementioned response arises mainly from the lowest multipolar order, as is indeed corroborated for the particular cases that were examined. The fields in the radiation zone can be synthesized as originating from an effective magnetic dipole oriented perpendicularly to the meridional plane and an effective electric dipole that lies in the meridional plane; these sources are located at the center of the sphere. We derived general conditions for achieving null radiation in any direction that lies in the meridional plane. As a consequence, the directional radiation of the dipole-scatterer antenna is obtained. The projection of the effective electric dipole along a unit vector in the meridional plane and the effective magnetic dipole can, under certain conditions, give rise to a Huygens dipole, obtaining null radiation in one of the directions of the normal vector to the plane expanded by such a unit vector and a vector parallel to the effective magnetic dipole. The remaining component of the effective electric dipole (parallel to the normal vector) influences the radiation pattern, and consequently, the directivity D as well. In addition, we have analyzed, in the far field, the spin angular momentum which can be seen as arising from the mixing among the effective dipoles.

We analyzed in detail the radiative characteristics and looked for geometrical and material (nonabsorbing) parameters of the dipole-scatterer antenna in which radiation vanishes unidirectionally along two particular axes: diagonal and principal. We were able to find specific parameters of the dipole-scatterer setup for which the aforementioned conditions were matched exactly. The flipping of the spinning direction of the circular dipole rotates the radiation and spin

patterns π rad around the axis that joins the position of the circular dipole and the center of the scatterer. As a consequence, when radiation nullifies in either of the forward or backward directions, these patterns are unaffected by the handedness of the circular dipole. The directivity curves D are bounded and depend on the angular direction in which radiation vanishes. Thus, the dipolar contribution of the radiation pattern coincides with the ideal case; the radiated power and radiation and spin patterns are practically unperturbed by high-order modes. For a given direction of null radiation, the shape of the spin pattern is independent of the relative strength of effective dipoles p_z and p_x .

We expect that this study might impact aspects related to the coupling of quantum spin states and electromagnetic modes, the control of radiation by emitters, the routing of light in networks, the manipulation of light by metasurfaces, and the sensing and localization of molecules.

APPENDIX A: ELECTRIC FIELD THAT IS GENERATED BY THE CIRCULAR DIPOLE

In general, the direct electric field that is created by an arbitrary electric dipole \mathbf{p} is

$$\mathbf{E}_0(\mathbf{r}) = [k_1^2/(\epsilon_0\epsilon_1)] \vec{\mathbf{G}}_0(\mathbf{r}, \mathbf{r}_0, \omega) \cdot \mathbf{p}. \quad (\text{A1})$$

Here, \mathbf{r}_0 is the dipole position, $\vec{\mathbf{G}}_0$ is the unbounded Green tensor whose multipolar expansion for $|\mathbf{r}| > |\mathbf{r}_0|$ is [34]

$$\begin{aligned} \vec{\mathbf{G}}_0(\mathbf{r}, \mathbf{r}_0, \omega) = ik_1 \sum_{\sigma lm} a_{lm} [\overline{\mathbf{M}}_{\sigma lm}(\mathbf{r}, k_1) \widehat{\mathbf{M}}_{\sigma lm}(\mathbf{r}_0, k_1) \\ + \overline{\mathbf{N}}_{\sigma lm}(\mathbf{r}, k_1) \widehat{\mathbf{N}}_{\sigma lm}(\mathbf{r}_0, k_1)], \end{aligned} \quad (\text{A2})$$

where

$$a_{lm} = \frac{1}{2\pi(1 + \delta_{0m})} \frac{(2l+1)(l-m)!}{l(l+1)(l+m)!}, \quad (\text{A3})$$

δ_{ij} is the δ -Kronecker tensor, and the summation indices run over $0 \leq m \leq l$ and $l = 1, 2, \dots$ (we recall that $\sigma = e, o$). Here, the vector spherical harmonic $\widehat{\mathbf{M}}_{\sigma lm}(\mathbf{r}, k)$ is defined as (3), but $h_l(kr)$ is replaced by $j_l(kr)$ and $\widehat{\mathbf{N}}_{\sigma lm}(\mathbf{r}, k)$ is obtained from (4) with the replacement $\widehat{\mathbf{M}}_{\sigma lm}(\mathbf{r}, k) \rightarrow \widehat{\mathbf{M}}_{\sigma lm}(\mathbf{r}, k)$. Because of the fact that the multipolar expansion (A2) is valid for $|\mathbf{r}| > |\mathbf{r}_0|$, the vector spherical harmonics related to the field point \mathbf{r} have outgoing spherical Hankel functions, whereas the vector spherical harmonics for the source points contain regular spherical Bessel functions to avoid divergence at $\mathbf{r}_0 = \mathbf{0}$. By considering the dipole position $\mathbf{r}_0 = z_0\mathbf{n}_z$, the projections of the right-hand vector spherical harmonics of Green tensor (A2) with unit vectors \mathbf{n}_x and \mathbf{n}_z [related to polarization of the circular dipole (1)] turn out to be

$$\widehat{\mathbf{N}}_{\sigma lm}(z_0\mathbf{n}_z, k) \cdot \mathbf{n}_x = \delta_{1m}\delta_{e\sigma} l(l+1) \psi'_l(kz_0)/(2kz_0), \quad (\text{A4})$$

$$\widehat{\mathbf{N}}_{\sigma lm}(z_0\mathbf{n}_z, k) \cdot \mathbf{n}_z = \delta_{0m}\delta_{e\sigma} l(l+1) \psi'_l(kz_0)/(kz_0), \quad (\text{A5})$$

$$\widehat{\mathbf{M}}_{\sigma lm}(z_0\mathbf{n}_z, k) \cdot \mathbf{n}_x = \delta_{1m}\delta_{o\sigma} l(l+1) j_l(kz_0)/2, \quad (\text{A6})$$

$$\widehat{\mathbf{M}}_{\sigma lm}(z_0\mathbf{n}_z, k) \cdot \mathbf{n}_z = 0. \quad (\text{A7})$$

These projections lead straightforwardly to the expression for the electric field given by (2).

The scattered electric field \mathbf{E}_s (outside the scatterer), which is generated by an arbitrary dipole \mathbf{p} , can be obtained also from (A1), but $\vec{\mathbf{G}}_0$ is replaced by the scattering Green tensor $\vec{\mathbf{G}}_s$ which admits also a multipolar expansion with respect to the origin as [35]

$$\begin{aligned} \vec{\mathbf{G}}_s(\mathbf{r}, \mathbf{r}_0, \omega) = & ik_1 \sum_{\sigma lm} a_{lm} [A_l(\omega) \overline{\mathbf{M}}_{\sigma lm}(\mathbf{r}, k_1) \\ & \times \overline{\mathbf{M}}_{\sigma lm}(\mathbf{r}_0, k_1) + B_l(\omega) \overline{\mathbf{N}}_{\sigma lm}(\mathbf{r}, k_1) \\ & \times \overline{\mathbf{N}}_{\sigma lm}(\mathbf{r}_0, k_1)]. \end{aligned} \quad (\text{A8})$$

Equation (6), that is, the particular expression for scattered electric field \mathbf{E}_s , is obtained from the scattering Green tensor (A8), but now the projections $\overline{\mathbf{N}}_{\sigma lm}(z_0 \mathbf{n}_z, k) \cdot \mathbf{n}_x$, $\overline{\mathbf{N}}_{\sigma lm}(z_0 \mathbf{n}_z, k) \cdot \mathbf{n}_z$, $\overline{\mathbf{M}}_{\sigma lm}(z_0 \mathbf{n}_z, k) \cdot \mathbf{n}_x$, and $\overline{\mathbf{M}}_{\sigma lm}(z_0 \mathbf{n}_z, k) \cdot \mathbf{n}_z$ are needed; they correspond respectively to the right-hand side of (A4)–(A7) with replacements $\psi'_l(kz_0) \rightarrow \xi'_l(kz_0)$ and $j_l(kz_0) \rightarrow h_l(kz_0)$. Since the domain of the scattering Green tensor (A8) is $|\mathbf{r}| > a$ and $|\mathbf{r}_0| > a$, both vector spherical harmonics of the dyadic possess outgoing spherical Hankel functions.

APPENDIX B: MULTIPOLAR CONTRIBUTIONS OF THE RADIATION PATTERN

The multipolar term of the radiation pattern $P_0^{-1}(dP_{ll'}/d\Omega)$ is defined as

$$\begin{aligned} \frac{1}{P_0} \frac{dP_{ll'}}{d\Omega} = & \frac{3}{8\pi} \text{Re} \left\{ \frac{-i}{2} \frac{(2l+1)}{(-i)^l l(l+1)} \frac{(2l'+1)}{i^{l'} l'(l'+1)} \right. \\ & \times [i\alpha_l^*(k_1 z_0) \alpha_{l'}(k_1 z_0) (\tau_l^1(\theta) \tau_{l'}^1(\theta) \sin^2 \phi \\ & + \Pi_l^1(\theta) \Pi_{l'}^1(\theta) \cos^2 \phi) - \alpha_l^*(k_1 z_0) \beta_{l'}(k_1 z_0) \\ & \times (\Pi_l^1(\theta) \tau_{l'}^1(\theta) \cos^2 \phi + \tau_l^1(\theta) \Pi_{l'}^1(\theta) \sin^2 \phi) \\ & \mp i l'(l'+1) \alpha_l^*(k_1 z_0) \gamma_{l'}(k_1 z_0) \Pi_l^1(\theta) \tau_{l'}^0(\theta) \cos \phi \end{aligned}$$

$$\begin{aligned} & + \beta_l^*(k_1 z_0) \alpha_{l'}(k_1 z_0) (\tau_l^1(\theta) \Pi_{l'}^1(\theta) \cos^2 \phi \\ & + \Pi_l^1(\theta) \tau_{l'}^1(\theta) \sin^2 \phi) + i \beta_l^*(k_1 z_0) \beta_{l'}(k_1 z_0) \\ & \times (\tau_l^1(\theta) \tau_{l'}^1(\theta) \cos^2 \phi + \Pi_l^1(\theta) \Pi_{l'}^1(\theta) \sin^2 \phi) \\ & \mp l'(l'+1) \beta_l^*(k_1 z_0) \gamma_{l'}(k_1 z_0) \tau_l^1(\theta) \cos \theta \tau_{l'}^0(\theta) \\ & \times \cos \phi \mp i l(l+1) \gamma_l^*(k_1 z_0) \alpha_{l'}(k_1 z_0) \\ & \times \tau_l^0(\theta) \Pi_{l'}^1(\theta) \cos \phi \pm l(l+1) \gamma_l^*(k_1 z_0) \\ & \times \beta_{l'}(k_1 z_0) \tau_l^0(\theta) \tau_{l'}^1(\theta) \cos \phi + i l(l+1) \\ & \times l'(l'+1) \gamma_l^*(k_1 z_0) \gamma_{l'}(k_1 z_0) \\ & \left. \times \tau_l^0(\theta) \tau_{l'}^0(\theta) \right\}. \end{aligned} \quad (\text{B1})$$

APPENDIX C: MULTIPOLAR CONTRIBUTIONS OF THE SPIN PATTERN

The multipolar contribution $s_{ll'}$ of the spin pattern is explicitly given by

$$\begin{aligned} s_{ll'} = & s_0 \text{Im} \left[\frac{1}{(-i)^l} \frac{2l+1}{l(l+1)} \frac{1}{(-i)^{l'}} \frac{2l'+1}{l'(l'+1)} \right. \\ & \times \left\{ \sin \phi \cos \phi [\tau_l^1(\theta) \Pi_{l'}^1(\theta) - \Pi_l^1(\theta) \tau_{l'}^1(\theta)] \right. \\ & \times [\alpha_l^*(k_1 z_0) \alpha_{l'}(k_1 z_0) - \beta_l^*(k_1 z_0) \beta_{l'}(k_1 z_0)] \\ & + i \sin \phi \cos \phi [\tau_l^1(\theta) \tau_{l'}^1(\theta) - \Pi_l^1(\theta) \Pi_{l'}^1(\theta)] \\ & \times [\alpha_l^*(k_1 z_0) \beta_{l'}(k_1 z_0) + \beta_l^*(k_1 z_0) \alpha_{l'}(k_1 z_0)] \\ & \mp l'(l'+1) \sin \phi \tau_l^1(\theta) \tau_{l'}^0(\theta) \alpha_l^*(k_1 z_0) \gamma_{l'}(k_1 z_0) \\ & \pm i l'(l'+1) \sin \phi \Pi_l^1(\theta) \tau_{l'}^0(\theta) \beta_l^*(k_1 z_0) \gamma_{l'}(k_1 z_0) \\ & \pm l(l+1) \sin \phi \tau_l^0(\theta) \tau_{l'}^1(\theta) \gamma_l^*(k_1 z_0) \alpha_{l'}(k_1 z_0) \\ & \pm i l(l+1) \sin \phi \tau_l^0(\theta) \Pi_{l'}^1(\theta) \\ & \left. \times \gamma_l^*(k_1 z_0) \beta_{l'}(k_1 z_0) \right\}, \end{aligned} \quad (\text{C1})$$

where $s_0 = 3n_1 P_0 / (16\pi c\omega)$.

-
- [1] M. Kerker, D.-S. Wang, and C. L. Giles, Electromagnetic scattering by magnetic spheres, *J. Opt. Soc. Am.* **73**, 765 (1983).
- [2] J. M. Geffrin, B. García-Cámara, R. Gómez-Medina, P. Albella, L. S. Froufe-Pérez, C. Eyraud, A. Litman, R. Vaillon, F. González, M. Nieto-Vesperinas, J. J. Sáenz, and F. Moreno, Magnetic and electric coherence in forward- and back-scattered electromagnetic waves by a single dielectric subwavelength sphere, *Nat. Commun.* **3**, 1171 (2012).
- [3] Y. H. Fu, A. I. Kuznetsov, A. E. Miroshnichenko, Y. F. Yu, and B. Luk'yanchuk, Directional visible light scattering by silicon nanoparticles, *Nat. Commun.* **4**, 1527 (2013).
- [4] S. Person, M. Jain, Z. Lapin, J. J. Sáenz, G. Wicks, and L. Novotny, Demonstration of zero optical backscattering from single nanoparticles, *Nano Lett.* **13**, 1806 (2013).
- [5] M. Dubois, L. Leroi, Z. Raolison, R. Abdeddaïm, T. Antonakakis, J. de Rosny, A. Vignaud, P. Sabouroux, E. Georget, B. Larrat, G. Tayeb, N. Bonod, A. Amadon, F. Mauconduit, C. Poupon, D. Le Bihan, and S. Enoch, Kerker Effect in Ultrahigh-Field Magnetic Resonance Imaging, *Phys. Rev. X* **8**, 031083 (2018).
- [6] W. Liu and Y. S. Kivshar, Generalized Kerker effects in nanophotonics and meta-optics, *Opt. Express* **26**, 13085 (2018).
- [7] H. K. Shamkhi, K. V. Baryshnikova, A. Sayanskiy, P. Kapitanova, P. D. Terekhov, P. Belov, A. Karabchevsky, A. B. Evlyukhin, Y. Kivshar, and A. S. Shalin, Transverse Scattering and Generalized Kerker Effects in All-Dielectric Mie-Resonant Metaoptics, *Phys. Rev. Lett.* **122**, 193905 (2019).
- [8] A. I. Barreda, J. M. Saiz, F. González, F. Moreno, and P. Albella, Recent advances in high refractive index dielectric nanoantennas: Basic and applications, *AIP Advances* **9**, 040701 (2019).
- [9] P. Genevet, F. Capasso, F. Aieta, M. Khorasaninejad, and R. Devlin, Recent advances in planar optics: From plasmonic to dielectric metasurfaces, *Optica* **4**, 139 (2017).

- [10] I. Staude, T. Pertsch, and Y. S. Kivshar, All-dielectric resonant meta-optics lightens up, *ACS Photonics* **6**, 802 (2019).
- [11] L. Wei, N. Bhattacharya, and H. P. Urbach, Adding a spin to Kerker's condition: Angular tuning of directional scattering with design excitation, *Opt. Lett.* **42**, 1776 (2017).
- [12] A. Bag, M. Neugebauer, P. Woźniak, G. Leuchs, and P. Banzer, Transverse Kerker Scattering for Angstrom Localization of Nanoparticles, *Phys. Rev. Lett.* **121**, 193902 (2018).
- [13] P. Albella, T. Shibanuma, and S. A. Maier, Switchable directional scattering of electromagnetic radiation with sub-wavelength asymmetric silicon dimers, *Sci. Rep.* **5**, 18322 (2015).
- [14] T. Shibanuma, T. Matsui, T. Roschuk, J. Wojcik, P. Mascher, P. Albella, and S. A. Maier, Experimental demonstration of tunable directional scattering of visible light from all-dielectric asymmetric dimers, *ACS Photonics* **4**, 489 (2017).
- [15] A. I. Barreda, H. Saleh, A. Litman, F. González, J.-M. Geffrin, and F. Moreno, Electromagnetic polarization-controlled perfect switching effect with high-refractive-index dimers and the beam-splitter configuration, *Nat. Commun.* **8**, 13910 (2017).
- [16] A. I. Barreda, Y. Gutiérrez, J. M. Sanz, F. González, and F. Moreno, Light guiding and switching using eccentric core-shell symmetries, *Sci. Rep.* **7**, 11189 (2017).
- [17] B. Rolly, B. Stout, S. Bidault, and N. Bonod, Crucial role of the emitter-particle distance on the directivity of optical antennas, *Opt. Lett.* **36**, 3368 (2011).
- [18] B. Rolly, B. Stout, and N. Bonod, Boosting the directivity of optical antennas with magnetic and electric dipolar resonant particles, *Opt. Express* **20**, 20376 (2012).
- [19] B. Rolly, J.-M. Geffrin, R. Abdeddaim, B. Stout, and N. Bonod, Controllable emission of a dipolar source coupled with a magneto-dielectric resonant subwavelength scatterer, *Sci. Rep.* **3**, 3063 (2013).
- [20] A. F. Cihan, A. G. Curto, S. Raza, P. G. Kik, and M. L. Brongersma, Silicon Mie resonators for highly directional light emission from monolayer MoS₂, *Nat. Photonics* **12**, 284 (2018).
- [21] A. G. Curto, G. Volpe, T. H. Taminiau, M. P. Kreuzer, R. Quidant, and N. F. van Hulst, Unidirectional emission a quantum dot coupled to a nanoantenna, *Science* **329**, 930 (2010).
- [22] F. J. Rodríguez-Fortuño, G. Marino, P. Ginzburg, D. O'Connor, A. Martínez, G. A. Wurtz, and A. V. Zayats, Near-field interference for the unidirectional excitation of electromagnetic guided modes, *Science* **340**, 328 (2013).
- [23] B. le Feber, N. Rotenberg, and L. Kuipers, Nanophotonic control of circular dipole emission, *Nat. Commun.* **6**, 6695 (2015).
- [24] T. van Mechelen and Z. Jacob, Universal spin-momentum locking of evanescent waves, *Optica* **3**, 118 (2016).
- [25] M. F. Picardi, A. Manjavacas, A. V. Zayats, and F. J. Rodríguez-Fortuño, Unidirectional evanescent-wave coupling from circularly polarized electric and magnetic dipoles: An angular spectrum approach, *Phys. Rev. B* **95**, 245416 (2017).
- [26] M. F. Picardi, A. V. Zayats, and F. J. Rodríguez-Fortuño, Janus and Huygens Dipoles: Near-Field Directionality beyond Spin-Momentum Locking, *Phys. Rev. Lett.* **120**, 117402 (2018).
- [27] F. Zhang, J. Ren, L. Shan, X. Duan, Y. Li, T. Zhang, Q. Gong, and Y. Gu, Chiral cavity quantum electrodynamics with coupled nanophotonic structures, *Phys. Rev. A* **100**, 053841 (2019).
- [28] D. Martin-Cano, H. R. Haakh, and N. Rotenberg, Chiral emission into nanophotonic resonators, *ACS Photonics* **6**, 961 (2019).
- [29] F. Khosravi, C. L. Cortes, and Z. Jacob, Spin photonics in 3D whispering gallery mode resonators, *Opt. Express* **27**, 15846 (2019).
- [30] R. Mitsch, C. Sayrin, B. Albrecht, P. Schneeweiss, and A. Rauschenbeutel, Quantum state-controlled directional spontaneous emission of photons into a nanophotonic waveguide, *Nat. Commun.* **5**, 5713 (2014).
- [31] A. B. Young, A. C. T. Thijssen, D. M. Beggs, P. Androvitsaneas, L. Kuipers, J. G. Rarity, S. Hughes, and R. Oulton, Polarization Engineering in Photonic Crystal Waveguides for Spin-Photon Entanglers, *Phys. Rev. Lett.* **115**, 153901 (2015).
- [32] R. J. Coles, D. M. Price, J. E. Dixon, B. Royall, E. Clarke, P. Kok, M. S. Skolnick, A. M. Fox, and M. N. Makhonin, Chirality of nanophotonic waveguide with embedded quantum emitter for unidirectional spin transfer, *Nat. Commun.* **7**, 11183 (2016).
- [33] Q. Guo, T. Fu, J. Tang, D. Pan, S. Zhang, and H. Xu, Routing a Chiral Raman Signal Based on Spin-Orbit of Light, *Phys. Rev. Lett.* **123**, 183903 (2019).
- [34] C.-T. Tai, *Dyadic Green Functions in Electromagnetic Theory*, 2nd ed. (IEEE Press, Piscataway, NJ, 1994).
- [35] L.-W. Li, P.-S. Kooi, M.-S. Leong, and T.-S. Yeo, Electromagnetic dyadic Green's function in spherically multilayered media, *IEEE T. Microw. Theory* **42**, 2302 (1994).
- [36] J. A. Stratton, *Electromagnetic Theory* (McGraw-Hill, New York and London, 1941).
- [37] M. F. Picardi, K. Y. Bliokh, F. J. Rodríguez-Fortuño, F. Alpeggiani, and F. Nori, Angular momenta, helicity, and other properties of dielectric-fiber and metallic-wire modes, *Optica* **5**, 1016 (2018).
- [38] J. H. Crichton and P. L. Marston, The measurable distinction between the spin and orbital angular momenta of electromagnetic radiation, *Electron. J. Differ. Eq. Conf.* **04**, 37 (2000).
- [39] J. B. Pendry, A. J. Holden, D. J. Robbins, and W. J. Stewart, Magnetism from conductors and enhanced nonlinear phenomena, *IEEE T. Microw. Theory* **47**, 2075 (1999).
- [40] V. Yannopapas, Artificial magnetism and negative refractive index in three-dimensional metamaterials of spherical particles at near-infrared and visible frequencies, *Appl. Phys. A* **87**, 259 (2007).
- [41] M. Choi, S. H. Lee, Y. Kim, S. B. Kang, J. Shin, M. H. Kwak, K.-Y. Kang, Y.-H. Lee, N. Park, and B. Min, A terahertz material with unnaturally high refractive index, *Nature (London)* **470**, 369 (2011).